RESEARCH ARTICLE

Check for updates

A surface precleaning strategy intensifies the interface coupling of the Bi₂O₃/TiO₂ heterostructure for enhanced photoelectrochemical detection properties†

Yajun Pang, ‡[ab] Qiang Feng,‡[a] Zongkui Kou, *[b] Guangqing Xu, *[ac] Feng Gao,[a] Bo Wang,[a] Zhenghui Pan,[b] Jun Lv,[ac] Yong Zhang [ac] and Yucheng Wu [ac]

The interfacial coupling effect plays a crucial role in tailoring the photoelectrochemical performance of heterostructured photocatalysts. However, it is an urgent need but challenging to intensify the interfacial coupling effect of heterojunctions. Herein, we proposed the surface precleaning of n-type TiO_2 *via* a facile low-temperature hydrogenation to facilitate strong coupling with p-type Bi_2O_3 (Bi_2O_3/c-TiO_2) and thus disruptively accelerate the electron transfer and electron–hole pair separation. The comparative studies of uncleaned Bi_2O_3/TiO_2 and Bi_2O_3/c-TiO_2 heterostructures by X-ray photoelectron spectroscopy revealed an unneglected valence change and thus a highly strong coupling effect between Bi_2O_3 and the cleaned TiO_2 originating from a possible weakening role of the nitrogen species adsorbed on the surface of pristine TiO_2 for the interfacial coupling effect. When integrated into a photoelectrochemical sensor, Bi_2O_3/c-TiO_2 presented both significantly high detection photocurrent response and selectivity for organics in a buffer solution. The current response of the as-built Bi_2O_3/c-TiO_2 was two-fold higher than that of uncleaned Bi_2O_3/TiO_2 and was even almost five-fold that of bulk TiO_2. We believe that this work will provide new perspectives and insights into the construction of efficient heterojunctions for impressive applications in photoelectrochemical detection.

Introduction

Water and environmental issues are listed among the top ten problems facing humanity for the next 50 years, where wastewater pollution affects the water and environment in many ways; in particular, organic matter pollution in water has caused widespread concern.[1–3] It is essential to detect the pollution of organic compounds in water to improve the water quality and unburden the environment load. The traditional determination method of potassium dichromate oxidation has been widely used for a relatively long period.[4,5] However, some limitations still exist in this approach, including a long reflux time, low detection sensitivity, and secondary pollution.

Hence, a couple of investigations have been done to improve the detection of the organic matter pollutants in water. The past decade has witnessed an explosive interest in constructing photoelectrochemical sensors based on photocatalysts due to their excellent intrinsic properties, such as non-toxicity, high oxidation capacity, and low cost.[6–8] Impressively, Zhou and colleagues reported a new type of organic detector based on the photoelectrocatalytic activity of TiO_2 nanotube arrays (TiO_2 NTAs), which endow no any toxic oxidants.[9,10] The development of a novel photoelectrochemical sensor based on TiO_2 NTAs *via* constructing the relation between the photocurrent and organic concentration in water has become a research object in recent years.[11–16] However, due to the wide band gap of TiO_2 and fast recombination of photogenerated carriers, the efficiency of photoelectrochemical detection is still extremely limited.

Effective photogenerated charge pairs are generally believed to be the key factor affecting the performances of semiconductor-based photocatalysts, which however will be counteracted if heterostructure engineering is not taken into account. The construction of a heterojunction by rationally integrating the appropriate components and selecting a suitable band gap has been well proven as an effective method to both suppress the recombination of photogenerated electron–hole pairs and

[a] School of Materials Science and Engineering, and Key Laboratory of Advanced Functional Materials and Devices of Anhui Province, Hefei University of Technology, Hefei 230009, China. E-mail: gqxu1979@hfut.edu.cn

[b] Department of Materials Science and Engineering, National University of Singapore, Singapore 117574, Singapore. E-mail: msekz@nus.edu.sg

[c] China International S&T Cooperation Base for Advanced Energy and Environmental Materials, Hefei 230009, China

‡ These authors contributed equally to this work.

accelerate the transport of the photocarriers of TiO_2.[17–19] For example, Bi_2O_3-modified TiO_2 NTAs have been successfully constructed to realize the regulation of the photoelectrochemical reaction process of TiO_2 NTAs when applied as a photoelectrochemical sensor.[16,20] However, the large charge transport resistance in the photoelectrochemical detection process decreases the efficiency of the photoelectrochemical reaction on the Bi_2O_3/TiO_2 heterostructure. Therefore, the insufficient coupling function in the above-mentioned heterojunction urgently needs to be improved for further enhancing the photoelectrochemical detection efficiency.

Herein, we demonstrated the surface precleaning of n-type TiO_2 via a facile low-temperature hydrogenation to facilitate strong coupling with p-type Bi_2O_3 (Bi_2O_3/c-TiO_2) and thus disruptively accelerate the electron transfer and electron–hole pair separation. Specifically, the adsorbed nitrogen species on the surface of TiO_2 were found to weaken the coupling effect in the Bi_2O_3/TiO_2 heterojunction system. The strong coupling effect in Bi_2O_3/c-TiO_2 was demonstrated by obvious changes in the valence states of the Ti and Bi elements. Consequently, compared to the bulk Bi_2O_3/TiO_2 heterostructure, Bi_2O_3/c-TiO_2 as a photoelectrochemical sensor exhibited fast charge transfer and highly selected electrochemical surface reactions, resulting in both a high detection photocurrent response and selectivity for organic targets in a buffer solution. The complicated coupling mechanism was also systematically investigated and discussed.

Experimental

Chemicals and sample preparation

Ti foils with a purity of 99.7% were purchased from Cuibolin (Beijing). Ethylene glycol, ammonium fluoride, disodium hydrogen phosphate (Na_2HPO_4), sodium dihydrogen phosphate (NaH_2PO_4), and absolute ethanol were purchased from Sinopharm Chemical Reagent.

Before anodization, the Ti foil was washed in acetone, DI water, and ethanol for 20 minutes each. TiO_2 NTAs were fabricated via two-step anodization. First, in a self-made double-electrode cell, the Ti foil with a diameter of 2.5 cm was anodized at a voltage of 60 V for 2 h. Specifically, in glycol solution containing 0.15 M NH_4F and 5 vol% H_2O, a graphite plate was used as the counter electrode and the Ti foil was used as the working electrode. Then, the obtained TiO_2 layer was cleared by ultrasonication in DI water for 10 min. The second anodization was performed at the same voltage of 60 V with the anodization time of 6 h. Finally, the products were ultrasonically cleaned in ethylene glycol to remove the broken nanotubes covered on the top surface of TiO_2 NTAs and then dried in an oven at 60 °C. The crystallization of the as-obtained amorphous TiO_2 was achieved by annealing at 500 °C for 2 h in air.

The two-step anodization of TiO_2 NTAs and the following preparation process are illustrated in Fig. 1. Precleaned TiO_2 NTAs (c-TiO_2 NTAs) were obtained by a low-temperature hydrogen thermal annealing method, in which TiO_2 was placed in a tube furnace and heated to 300 °C in a hydrogen environment at a heating rate of 1 °C min^{-1} for 4 h. Bi_2O_3 was loaded on c-TiO_2 NTAs by an ultrasonication-assisted successive ionic layer
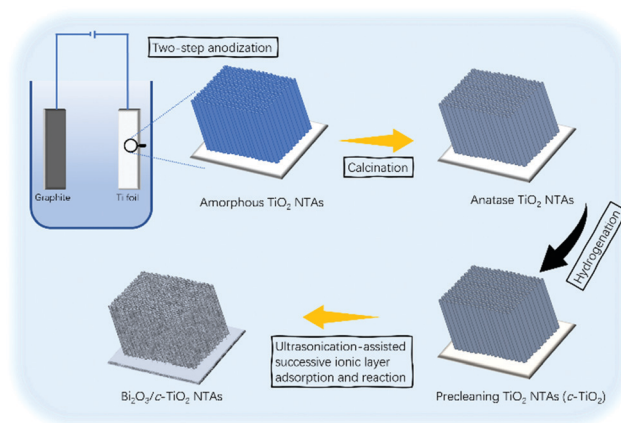

Fig. 1 Schematic illustration for the preparation of Bi_2O_3/c-TiO_2 NTAs.

adsorption and reaction strategy. First, the treated TiO_2 was soaked in a 10 mM $Bi(NO_3)_3\cdot5H_2O$ ethylene glycol solution and a 0.1 M NaOH ethanol solution for 10 minutes, respectively, using an ultrasonic generator. The product was then thoroughly rinsed in ethanol to remove any residual solution between each soaking step. This operation was repeated for 3 cycles. Then, the products were dried in an oven and annealed at 500 °C for 2 h in a tube furnace at a heating rate of 5 °C min^{-1}.

Characterization

The phase structures of the products were analyzed by using X-ray diffraction (XRD) with Cu-Kα radiation (D/MAX2500V). The morphologies were characterized by using field emission scanning electron microscopy (FE-SEM, SU8020) and high-resolution transmission electron microscopy (HR-TEM, JEOL JEM-2100F). The elemental composition of the samples was investigated by X-ray photoelectron spectroscopy (XPS, CALAB250) using Al Kα monochromatized radiation. Photoluminescence (PL) spectra were obtained on an F-4500 fluorescence spectrophotometer. UV-vis optical absorption was recorded by using a Hitachi UV-3600 spectrophotometer (Japan), and $BaSO_4$ was used as a reference.

Photoelectrochemical measurements

The photoelectrochemical performances were evaluated in a self-made circulatory system using a CHI660D electrochemical workstation.[16] The obtained nanotube arrays were used as the working electrode. A 3 M KCl saturated Ag/AgCl electrode and a Pt electrode were used as the reference electrode and counter electrode, respectively. The supporting electrolyte was 0.05 M phosphate buffer solution having a pH of 7 by adjusting the ratio of Na_2HPO_4 to NaH_2PO_4. A UV LED was used as the light source with a spot diameter of 10 mm, fixed wavelength at 365 nm, and adjustable optical power from 0 to 1200 mW cm^{-2} (an optical power of 4% was applied in this study).

Results and discussion

To explore the difference in the morphologies of these samples, Fig. 2a–c and Fig. S1 (ESI†) show the SEM images of TiO_2, c-TiO_2,
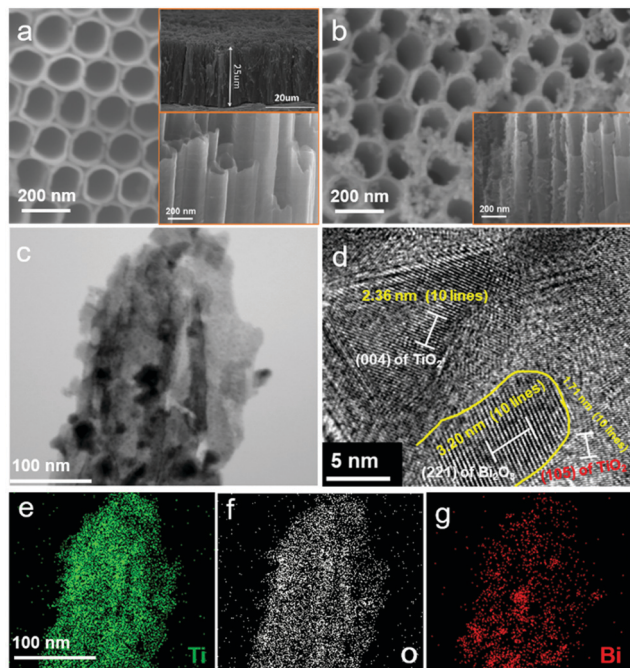
This journal is © The Royal Society of Chemistry and the Chinese Chemical Society 2020

Mater. Chem. Front., 2020, **4**, 638–644 | **639**

Fig. 2 Morphology and structural characterization. (a and b) SEM images of TiO₂ and Bi₂O₃/c-TiO₂ NTAs. The corresponding insets show cross-sectional images. (c–g) TEM images at different magnifications and the corresponding EDS element mapping images of Ti, Bi, and O for Bi₂O₃/c-TiO₂ NTAs.

and Bi₂O₃/c-TiO₂ NTAs. A large area of highly ordered nanotube arrays can be observed in the SEM image for the as-synthesized TiO₂ (Fig. S1a, ESI†). The c-TiO₂ showed similar morphology to that of the as-received TiO₂ NTAs with high density and a well-ordered and uniform tubular structure (Fig. 2a and Fig. S1b, ESI†), indicating that there was no obvious change in the surface morphology after the hydrogen thermal treatment. Moreover, with the ultrasonication-assisted method, ultra-small-sized Bi₂O₃ was successfully deposited on c-TiO₂ NTAs (Fig. 2b). In addition, the controlled introduction of Bi₂O₃ could be simply achieved by regulating the cycle of the deposition process (see SEM images in Fig. S1c, ESI† and Fig. 2b). The TEM image of Bi₂O₃/c-TiO₂ NTAs is shown in Fig. 2c, where Bi₂O₃ with an ultra-small size can be observed to be evenly deposited on TiO₂ NTAs. As observed in the high-resolution TEM image (Fig. 2d), the typical lattice spacings of 0.236 nm, 0.171 nm, and 0.320 nm correspond to the (111) and (105) planes of the TiO₂ anatase phase (JCPDS file No. 21-1272) and the (221) plane of Bi₂O₃ (JCPDS file No. 29-0236).[21–23] The corresponding EDS element mapping (Fig. 2e–g) demonstrates that the as-prepared Bi₂O₃ is highly dispersed on the c-TiO₂ nanotubes. Specifically, except for the Ti and O elements, the as-built Bi₂O₃/c-TiO₂ sample has an atomic Bi percentage of about 5.89% (Fig. S1d, ESI†).

The crystal structures and phases of all the studied samples were identified by XRD patterns and Raman spectra. As displayed in Fig. 3a, c-TiO₂ NTAs show similar diffraction peaks to those of TiO₂ NTAs. The diffraction peaks at 25.36° and 37.91° for TiO₂ and c-TiO₂ NTAs can be well indexed to the (101) and (004) planes of the TiO₂ anatase phase (JCPDS file No. 21-1272),

respectively, indicating that the hydrogenation treatment did not change the phase and crystal properties of TiO₂ NTAs. The Bi₂O₃/c-TiO₂ NTA sample showed some new peaks at the 2θ values of 27.46° and 44.96°, corresponding to the (310) and (431) planes of Bi₂O₃ (JCPDS file No. 29-0236).[23,24] Furthermore, in the Raman spectra (Fig. S3a, ESI†), no differences can be found between the peaks for TiO₂ and c-TiO₂, and these characteristic peaks at 141, 192, 392, 512, and 634 cm⁻¹ belong to anatase TiO₂. However, after Bi₂O₃ deposition, an obvious peak of Bi₂O₃/c-TiO₂ NTAs appeared at 309 cm⁻¹ due to the existence of Bi–O bonds with various bond lengths.[23] Both the XRD and Raman results demonstrated that Bi₂O₃ was successfully deposited on c-TiO₂ NTAs via such a facile ultrasonication-assisted method.

To further analyze the surfacial/interfacial chemical valence and coupling effect of the samples, the XPS survey spectra were performed. Two main peaks of O 1s and Ti 2p could be observed due to the existence of O and Ti, respectively, for all the samples (see the overall survey patterns in Fig. S3b, ESI†). First, the high-resolution spectra of N 1s for TiO₂ and c-TiO₂ were recorded to compare the surface functional groups. In the region of N 1s (Fig. 3b), there is almost no N 1s XPS peak in the measured spectrum of c-TiO₂, while it is evidently observed for pristine TiO₂. According to previous reports, the peak at ∼400.2 eV can be assigned to various adsorbed nitrogen-containing species.[25,26] Therefore, TiO₂ with clean surfaces was obtained by a low-temperature hydrogenation treatment. The comparison of the Ti 2p spectra of TiO₂ and c-TiO₂ NTAs (Fig. 3c) suggested no obvious binding energy shift. Moreover, unlike the unclean Bi₂O₃/TiO₂ sample, Bi₂O₃/c-TiO₂ NTAs presented an obvious shift in the Ti 2p peaks compared with TiO₂ NTAs, suggesting a strong interaction between the Ti atoms and the adjacent atoms.[27–29] A highly strong coupling between Bi₂O₃ and c-TiO₂ was thus established, which holds great potential for
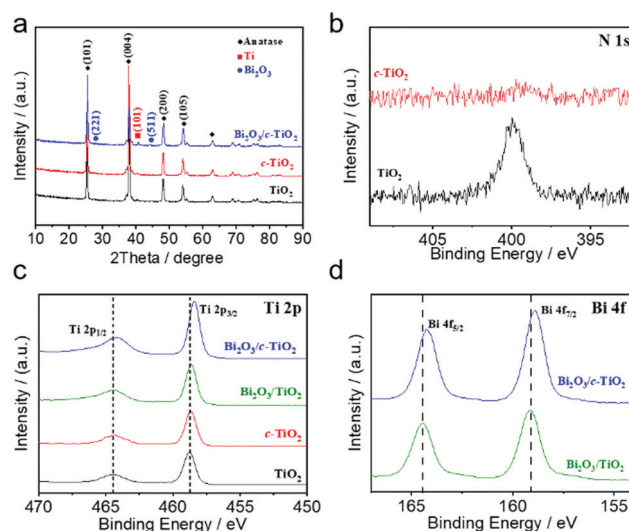

Fig. 3 Phase and surface termination species analysis of TiO₂, c-TiO₂, Bi₂O₃/TiO₂, and Bi₂O₃/c-TiO₂ NTAs. (a) XRD patterns. (b–d) High-resolution XPS spectra of N 1s, Ti 2p, and Bi 4f.

640 | Mater. Chem. Front., 2020, **4**, 638–644

This journal is © The Royal Society of Chemistry and the Chinese Chemical Society 2020

accelerating the electron transfer and electron–hole pair separation. Therefore, we can also conclude that the adsorbed radicals on the surface of semiconductors can weaken the coupling function between Bi_2O_3 and TiO_2, leading to an unexpected resistance enhancement in heterostructure engineering. Additionally, the high-resolution XPS spectra of Bi 4f in Bi_2O_3/TiO_2 and Bi_2O_3/c-TiO_2 are shown in Fig. 3d. Two peaks belonging to Bi $4f_{7/2}$ and Bi $4f_{5/2}$ can be observed. Obviously, the binding energy for Bi_2O_3/c-TiO_2 NTAs presented a negative shift of ~ 0.2 eV when compared to that for Bi_2O_3/TiO_2 NTAs, further demonstrating the strong coupling effect in the as-synthesized Bi_2O_3/c-TiO_2 NTAs. In order to further confirm the stability of the strong coupling, the high-resolution Ti 2p and Bi 4f XPS spectra of Bi_2O_3/TiO_2 and Bi_2O_3/c-TiO_2 after detection tests for 10 cycles were measured (see Fig. S5, ESI†). Clearly, the Ti 2p and Bi 4f XPS spectra of Bi_2O_3/c-TiO_2 still presented a visible shift compared with that of Bi_2O_3/TiO_2, which confirmed the excellent stability of the strong coupling interaction.

When applied in the PEC detection of organics in aqueous solutions, the strength of the current response and selectivity between the base solution and organics are crucial for the construction of a high-performance PEC sensor. Thereby, curves for the background photocurrent (decomposition from a buffer solution) and relative current response to organics (decomposition from a 0.1 mM glucose target) were obtained by the amperometric method using a self-made flow-injection device at an applied potential of 0.2 V in a buffer solution (Fig. 4a and b).[16] On the one hand, by comparing the background photocurrents among the four samples, both TiO_2 and c-TiO_2 exhibited higher background photocurrents than Bi_2O_3/TiO_2 and Bi_2O_3/c-TiO_2, showing that the introduction of Bi_2O_3 suppressed the photolysis of water during the detection processes. Specifically, the background photocurrents of TiO_2, c-TiO_2, Bi_2O_3/TiO_2, and Bi_2O_3/c-TiO_2 NTAs were measured to be 136.82 μA, 261.63 μA, 57.83 μA, and 32.68 μA, respectively (Fig. 4b). A limited background photocurrent is beneficial to obtain efficient selectivity. On the other hand, it could be observed that the current responses to glucose of the corresponding four samples were 6.73 μA, 12.84 μA, 14.52 μA, and 29.12 μA, which suggested that both a low background current and enhanced current response were achieved for the Bi_2O_3/TiO_2 and Bi_2O_3/c-TiO_2 samples. Moreover, by comparing the performances of the heterostructure with and without precleaning, the enhanced coupling effect in Bi_2O_3/c-TiO_2 was seen to play a great role in enhancing the current response. Impressively, the as-prepared Bi_2O_3/c-TiO_2 exhibited a response two-fold higher than that of blank Bi_2O_3/TiO_2 and even 5 times that of bulk TiO_2.

To further determine the photoelectrochemical detection performance including the sensitivity, current detection noise, linear range and detection limit of the as-prepared samples, the photoelectrochemical performances of the as-assembled four samples were obtained via the step-by-step infusion of a glucose target (Fig. 4c). For convenient comparison, the current–time curves were moved to the same starting point. Obviously, the current increment of c-TiO_2, Bi_2O_3/TiO_2, and Bi_2O_3/c-TiO_2 went

Fig. 4 Photoelectrochemical properties of TiO_2, Bi_2O_3/TiO_2, c-TiO_2, and Bi_2O_3/c-TiO_2 NTAs. (a and b) Photocurrent and current response curves. (c and d) Current–time curves and plots of current increment vs. concentration. (e) Detection current noise. (f) Stability test.

faster than that for bulk TiO_2 with the same injection, indicating a higher response current to glucose, especially for Bi_2O_3/c-TiO_2 NTAs. Furthermore, plots of the current increment vs. detection concentration range were obtained by calculating from Fig. 4c, where the detection sensitivity and range could be obtained (Fig. 4d). The as-built Bi_2O_3/c-TiO_2 NTAs presented both highly improved sensitivity (0.214 μA μM^{-1}) and range (1185.5 μM) performances, which were much better than those of others. To vividly understand the influence of the background photocurrent on the photoelectrochemical detection of organics, the current noises of these samples with the first injection of glucose in the current–time curves are presented in Fig. 4e. The current noises of TiO_2, c-TiO_2, Bi_2O_3/TiO_2, and Bi_2O_3/c-TiO_2 were 0.812 μA, 0.431 μA, 0.669 μA, and 0.372 μA, respectively. In addition, the detection limit (dl) was obtained by the sensitivity and current noise data (dl = 3σ/m, where σ is the background current noise, and m is the slope of the linear part of the calibration curve).[12,30,31] The dl values of the corresponding samples were 27.68 μM, 8.73 μM, 12.39 μM, and 5.21 μM. The detailed determination performance parameters are listed in Table S1 (ESI†) for better comparison. The constructed Bi_2O_3/c-TiO_2 NTAs also presented superior stability (Fig. 4f). By comparison, we can conclude that the photoelectrochemical detector based on Bi_2O_3/c-TiO_2 NTAs presents superior detecting performances with the sensitivity of 0.214 μA μM^{-1}, detection limit of 5.21 μM, and linear range from 0 to 1185.8 μM, thus holding a greater potential than others.

In addition to the above-mentioned Bi_2O_3/c-TiO_2 due to the strong coupling effect, which is more favorable for the desorption

This journal is © The Royal Society of Chemistry and the Chinese Chemical Society 2020

Mater. Chem. Front., 2020, 4, 638–644 | 641

of organic decomposition products, the change in photo-electrochemical properties also has an important influence on the detection performance of organics. Therefore, all the complicated photoelectrochemical processes, including optical absorption, charge separation efficiency, transfer rate, and electrochemical surface reactions, are deeply discussed in the following section.

First, optical properties are the key factors for the photo-electrochemical performance, as shown in Fig. 5a; all the samples have excellent optical absorption properties in the UV range. Compared with pristine TiO_2 NTAs, c-TiO_2 showed improved absorption in both the UV and visible regions, as described in many previous reports. The light absorption decreased in the UV region with the introduction of Bi_2O_3; in particular, when taking into account the light wavelength (365 nm) used in this study, it could be found that the modification of Bi_2O_3 alone did not improve the light absorption performance. This may be due to the low content of Bi_2O_3 in TiO_2 or c-TiO_2. In other words, the reason for the superior photoelectrochemical detection performances was not attributed to the optical properties.

Second, the recombination rate and charge transfer rate of the photogenerated electron–hole pairs were studied by using the photoluminescence (PL) method with an excitation wavelength of 315 mm and electrochemical impedance spectra (EIS) with a range from 10^{-1} to 10^5 Hz at a voltage of 0.2 V, respectively (Fig. 5b and c).[32–34] On the one hand, by comparing

the PL intensity of the as-prepared samples, we found that (1) the introduction of Bi_2O_3 in both the samples could promote the separation of photogenerated charge carriers and (2) Bi_2O_3/c-TiO_2 exhibited strongly superior separation efficiency when compared with blank Bi_2O_3/TiO_2. On the other hand, obviously, the Nyquist plots for all four samples presented a similar shape but with different impendence arcs (Fig. 5c). In general, if the radius of the arc becomes smaller, it implies a fast charge transfer rate. The arc radius of c-TiO_2 was smaller than that of bulk TiO_2, indicating better conductivity after surface precleaning, which is consistent with the result of a significant enhancement in the background photocurrent of c-TiO_2 NTAs in a buffer solution. Impressively, higher charge transfer resistance of both Bi_2O_3/TiO_2 and Bi_2O_3/c-TiO_2 was obtained by the coupling of Bi_2O_3, indicating that the existence of Bi_2O_3 could not improve the conductivity for pristine TiO_2 and c-TiO_2 in this case. However, with the precleaning treatment of pristine TiO_2, the charge transfer resistance was reduced extremely, suggesting enhanced coupling between the heterostructured semiconductors in the Bi_2O_3/c-TiO_2 system, further resulting in highly enhanced photo-electrochemical detection properties.

Last but not the least, the electrochemical surface reaction plays a key role in enhancing the photoelectrochemical detection performances, including the direct oxidative decomposition of organic compounds by holes (h^+) and the indirect oxidation and decomposition of organic matter in water by •OH radicals.[16] Thereby, we investigated the change in the photocurrents of the four samples by adding trapping agents for holes and hydroxyl radicals, respectively (Fig. 5d and e). Ammonium oxalate (AO) and isopropanol (IPA) contributed to holes and hydroxyl radicals, respectively.[35,36] Clearly, the main active species for pristine TiO_2 and c-TiO_2 were still hydroxyl radicals, indicating that precleaning could not regulate the electrochemical surface reactions of TiO_2. However, for Bi_2O_3-containing TiO_2 and c-TiO_2, the holes became the main active species during the PEC processes. Considering that the introduction of Bi_2O_3 could enhance the detection response, the holes were more efficient in the decomposition of organics when compared with the hydroxyl radicals. We further proved the intensity of hydroxyl radicals in samples by testing the fluorescence density of 2-hydroxyterephthalic acid when excited by light with a wavelength of 315 nm, which is the product of the reaction of terephthalic acid with hydroxyl radicals (Fig. 5f),[37,38] further supporting the trapping agent results. The emission intensities of Bi_2O_3/TiO_2 and Bi_2O_3/c-TiO_2 NTAs were lower than those of the two pristine samples, confirming the lower productivity of hydroxyl radicals. Clearly, it was demonstrated that the detection action by holes is more advantageous to the PEC detection performances in comparison with the detection by hydroxyl radicals when considering the electrochemical surface reactions.
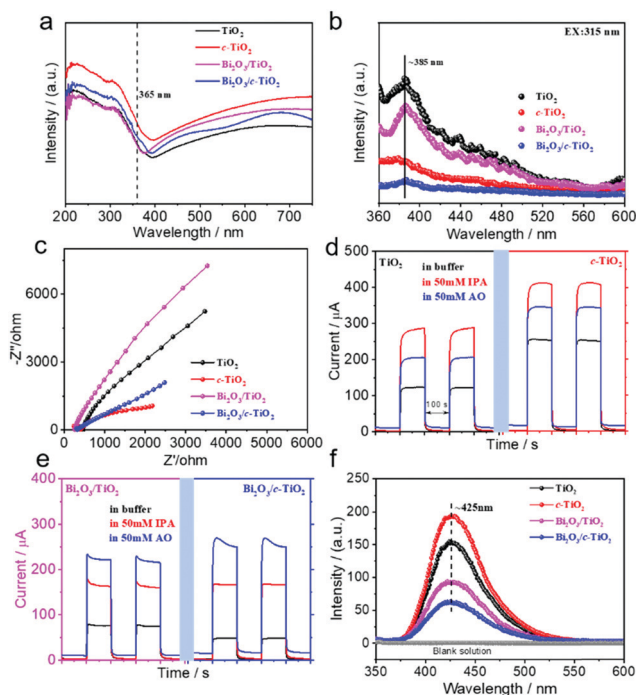

Fig. 5 Optical properties and electrochemical surface reactions of the as-prepared samples. (a) UV-Vis absorption spectra. (b) PL spectra. (c) EIS spectra. (d and e) Trapping experiment for holes and hydroxyl radicals. (f) PL spectra of terephthalic acid after being illuminated under UV light with TiO_2, c-TiO_2, Bi_2O_3/TiO_2, and Bi_2O_3/c-TiO_2 NTAs for 30 min.

Conclusions

In summary, we exploited an effective surface precleaning approach to enhance the performance of a photoelectrochemical (PEC) sensor for the detection of organics by intensifying the

coupling effect between Bi_2O_3 and precleaned TiO_2 (Bi_2O_3/c-TiO_2). In comparison with the current response of the unclean Bi_2O_3/TiO_2 heterostructure, the current response of the as-built Bi_2O_3/c-TiO_2 was enhanced by two-fold, which was even five-fold that of bulk TiO_2. Impressively, we revealed the negative role of the nitrogen-containing radicals adsorbed on the surface of TiO_2 in constructing the high-performance heterojunction system. Specifically, the photoelectrochemical detector based on Bi_2O_3/c-TiO_2 NTAs presented superior detecting performances, *e.g.*, sensitivity, detection limit, and linear range, thus holding the greatest potential among TiO_2, c-TiO_2, and Bi_2O_3/TiO_2 NTAs originating from the accelerated photogenerated charge transfer and proper regulated electrochemical surface reactions by intensifying the interfacial coupling effect.

Conflicts of interest

There are no conflicts to declare.

Acknowledgements

Notes and references

1 R. E. Smalley, *Energy & NanoTechnology Conference*, Rice University, 2003.

2 D. Yue, X. Qian, M. Kan, M. Fang, J. Jia, X. Yang and Y. Zhao, A metal-free visible light active photo-electro-Fenton-like cell for organic pollutants degradation, *Appl. Catal., B*, 2018, **229**, 211–217.

3 Y. Qiu, Z. Pan, H. Chen, D. Ye, G. Lin, Z. Fan and S. Yang, Current progress in developing metal oxide nanoarrays-based photoanodes for photoelectrochemical water splitting, *Sci. Bull.*, 2019, **64**, 1348–1380.

4 M. Kolb, M. Bahadir and B. Teichgräber, Determination of chemical oxygen demand (COD) using an alternative wet chemical method free of mercury and dichromate, *Water Res.*, 2017, **122**, 645–654.

5 C. E. Domini, M. Hidalgo, F. Marken and A. Canals, Comparison of three optimized digestion methods for rapid determination of chemical oxygen demand: closed microwaves, open microwaves and ultrasound irradiation, *Anal. Chim. Acta*, 2006, **561**, 210–217.

6 Y. Han, S. Zhang, H. Zhao, W. Wen, H. Zhang, H. Wang and F. Peng, Photoelectrochemical characterization of a robust TiO_2/BDD heterojunction electrode for sensing application in aqueous solutions, *Langmuir*, 2009, **26**, 6033–6040.

7 S. Li, J. Qiu, M. Ling, F. Peng, B. Wood and S. Zhang, Photoelectrochemical characterization of hydrogenated TiO_2 nanotubes as photoanodes for sensing applications, *ACS Appl. Mater. Interfaces*, 2013, **5**, 11129–11135.

8 X. Wang, X. Xia, X. Zhang, W. Meng, C. Yuan and M. Guo, Nonenzymatic glucose sensor based on Ag&Pt hollow nanoparticles supported on TiO_2 nanotubes, *Mater. Sci. Eng., C*, 2017, **80**, 174–179.

9 Q. Zheng, B. Zhou, J. Bai, L. Li, Z. Jin, J. Zhang, J. Li, Y. Liu, W. Cai and X. Zhu, Self-organized TiO_2 nanotube array sensor for the determination of chemical oxygen demand, *Adv. Mater.*, 2008, **20**, 1044–1049.

10 L. Bingchuan, L. Jinhua, Z. Baoxue, Q. Zheng, B. Jing, J. Zhang, L. Yanbiao and C. Weimin, Kinetics and mechanisms for photoelectrochemical degradation of glucose on highly effective self-organized TiO_2 nanotube arrays, *Chin. J. Catal.*, 2010, **31**, 163–170.

11 J. Bai and B. Zhou, Titanium dioxide nanomaterials for sensor applications, *Chem. Rev.*, 2014, **114**, 10131–10176.

12 Y. Pang, G. Xu, X. Zhang, J. Lv, K. Shi, P. Zhai, Q. Xue, X. Wang and Y. Wu, Photoelectrochemical properties and the detection mechanism of Bi_2WO_6 nanosheet modified TiO_2 nanotube arrays, *Dalton Trans.*, 2015, **44**, 17784–17794.

13 C. Liu, H. Zhao, Z. Ma, T. An, C. Liu, L. Zhao, D. Yong, J. Jia, X. Li and S. Dong, Novel environmental analytical system based on combined biodegradation and photoelectrocatalytic detection principles for rapid determination of organic pollutants in wastewaters, *Environ. Sci. Technol.*, 2014, **48**, 1762–1768.

14 L. Li, T. Wang, Y. Zhang, C. Xu, L. Zhang, X. Cheng, H. Liu, X. Chen and J. Yu, Editable TiO_2 nanomaterial-modified paper in situ for highly efficient detection of carcinoembryonic antigen by photoelectrochemical method, *ACS Appl. Mater. Interfaces*, 2018, **10**, 14594–14601.

15 H. Si, N. Pan, X. Zhang, J. Liao, M. Rumyantseva, A. Gaskov and S. Lin, A real-time on-line photoelectrochemical sensor toward chemical oxygen demand determination based on field-effect transistor using an extended gate with 3D TiO_2 nanotube arrays, *Sens. Actuators, B*, 2019, **289**, 106–113.

16 Y. Pang, Y. Li, G. Xu, Y. Hu, Z. Kou, Q. Feng, J. Lv, Y. Zhang, J. Wang and Y. Wu, Z-scheme carbon-bridged Bi_2O_3/TiO_2 nanotube arrays to boost photoelectrochemical detection performance, *Appl. Catal., B*, 2019, **248**, 255–263.

17 W. Wang, S. Zhu, Y. Cao, Y. Tao, X. Li, D. Pan, D. L. Phillips, D. Zhang, M. Chen and G. Li, Edge-Enriched Ultrathin MoS_2 Embedded Yolk–Shell TiO_2 with Boosted Charge Transfer for Superior Photocatalytic H_2 Evolution, *Adv. Funct. Mater.*, 2019, **29**, 1901958.

18 Z. Tian, P. Zhang, P. Qin, D. Sun, S. Zhang, X. Guo, W. Zhao, D. Zhao and F. Huang, Novel Black $BiVO_4/TiO_{2-x}$ Photoanode with Enhanced Photon Absorption and Charge Separation for Efficient and Stable Solar Water Splitting, *Adv. Energy Mater.*, 2019, 1901287.

19 F. Wu, Y. Yu, H. Yang, L. N. German, Z. Li, J. Chen, W. Yang, L. Huang, W. Shi and L. Wang, Simultaneous enhancement of charge separation and hole transportation in a TiO_2–$SrTiO_3$

This journal is © The Royal Society of Chemistry and the Chinese Chemical Society 2020

Mater. Chem. Front., 2020, **4**, 638–644 | 643

core–shell nanowire photoelectrochemical system, *Adv. Mater.*, 2017, **29**, 1701432.

20 Y. Pang, G. Xu, C. Fan, J. Lv, J. Liu and Y. Wu, Photo-electrochemical detection performance and mechanism discussion of Bi_2O_3 modified TiO_2 nanotube arrays, *RSC Adv.*, 2016, **6**, 61367–61377.

21 Y. Li, Y. Huang, C. Ou, J. Zhu, X. Yuan, L. Yan, W. Li and H. Zhang, Enhanced capability and cyclability of flexible TiO_2-reduced graphene oxide hybrid paper electrode by incorporating monodisperse anatase TiO_2 quantum dots, *Electrochim. Acta*, 2018, **259**, 474–484.

22 Y. Zhang, J. Chen, H. Tang, Y. Xiao, S. Qiu, S. Li and S. Cao, Hierarchically-structured SiO_2–Ag@TiO_2 hollow spheres with excellent photocatalytic activity and recyclability, *J. Hazard. Mater.*, 2018, **354**, 17–26.

23 M. Ge, C. Cao, S. Li, S. Zhang, S. Deng, J. Huang, Q. Li, K. Zhang, S. S. Al-Deyab and Y. Lai, Enhanced photocatalytic performances of n-TiO_2 nanotubes by uniform creation of p–n heterojunctions with p-Bi_2O_3 quantum dots, *Nanoscale*, 2015, **7**, 11552–11560.

24 X. Guo, C. Lai, X. Jiang, W. Mi, X. Yin, X. Li and Y. Shu, Remarkably facile fabrication of extremely superhydrophobic high-energy binary composite with ultralong lifespan, *Chem. Eng. J.*, 2018, **335**, 843–854.

25 T. Ma, M. Akiyama, E. Abe and I. Imai, High-efficiency dye-sensitized solar cell based on a nitrogen-doped nanostructured titania electrode, *Nano Lett.*, 2005, **5**, 2543–2547.

26 T. Boningari, S. N. R. Inturi, M. Suidan and P. G. Smirniotis, Novel one-step synthesis of nitrogen-doped TiO_2 by flame aerosol technique for visible-light photocatalysis: effect of synthesis parameters and secondary nitrogen (N) source, *Chem. Eng. J.*, 2018, **350**, 324–334.

27 J. Tao, J. Chai, L. Guan, J. Pan and S. Wang, Effect of interfacial coupling on photocatalytic performance of large scale MoS_2/TiO_2 hetero-thin films, *Appl. Phys. Lett.*, 2015, **106**, 081602.

28 P. Scheiderer, F. Pfaff, J. Gabel, M. Kamp, M. Sing and R. Claessen, Surface-interface coupling in an oxide hetero-structure: impact of adsorbates on $LaAlO_3$/$SrTiO_3$, *Phys. Rev. B: Condens. Matter Mater. Phys.*, 2015, **92**, 195422.

29 F. Nan, P. Li, J. Li, T. Cai, S. Ju and L. Fang, Experimental and Theoretical Evidence of Enhanced Visible Light Photo-electrochemical and Photocatalytic Properties in MoS_2/TiO_2 Nanohole Arrays, *J. Phys. Chem. C*, 2018, **122**, 15055–15062.

30 H. Liu, Y. Ding, B. Yang, Z. Liu, Q. Liu and X. Zhang, Colorimetric and ultrasensitive detection of H_2O_2 based on Au/Co_3O_4-CeO_x nanocomposites with enhanced peroxidase-like performance, *Sens. Actuators, B*, 2018, **271**, 336–345.

31 Y. Haldorai, S. R. Choe, Y. S. Huh and Y.-K. Han, Metal-organic framework derived nanoporous carbon/Co_3O_4 composite electrode as a sensing platform for the determination of glucose and high-performance supercapacitor, *Carbon*, 2018, **127**, 366–373.

32 J. Liu, W. Fang, Z. Wei, Z. Qin, Z. Jiang and W. Shangguan, Efficient photocatalytic hydrogen evolution on N-deficient g-C_3N_4 achieved by a molten salt post-treatment approach, *Appl. Catal., B*, 2018, **238**, 465–470.

33 Y. Pang, G. Xu, Q. Feng, J. Liu, J. Lv, Y. Zhang and Y. Wu, Synthesis of α-$Bi_2Mo_3O_{12}$/TiO_2 Nanotube Arrays for Photo-electrochemical COD Detection Application, *Langmuir*, 2017, **33**, 8933–8942.

34 X. Li, K. Zhang, D. Mitlin, Z. Yang, M. Wang, Y. Tang, F. Jiang, Y. Du and J. Zheng, Fundamental insight into Zr modification of Li-and Mn-rich cathodes: combined transmission electron microscopy and electrochemical impedance spectroscopy study, *Chem. Mater.*, 2018, **30**, 2566–2573.

35 S. Li, S. Hu, W. Jiang, Y. Liu, Y. Zhou, J. Liu and Z. Wang, Facile synthesis of cerium oxide nanoparticles decorated flower-like bismuth molybdate for enhanced photocatalytic activity toward organic pollutant degradation, *J. Colloid Interface Sci.*, 2018, **530**, 171–178.

36 S. Xiao, W. Dai, X. Liu, D. Pan, H. Zou, G. Li, G. Zhang, C. Su, D. Zhang and W. Chen, Microwave-Induced Metal Dissolution Synthesis of Core–Shell Copper Nanowires/ZnS for Visible Light Photocatalytic H_2 Evolution, *Adv. Energy Mater.*, 2019, **9**, 1900775.

37 D. Mao, J. Yuan, X. Qu, C. Sun, S. Yang and H. He, Size tunable Bi_3O_4Br hierarchical hollow spheres assembled with {001}-facets exposed nanosheets for robust photo-catalysis against phenolic pollutants, *J. Catal.*, 2019, **369**, 209–221.

38 C. Zhou, S. Wang, Z. Zhao, Z. Shi, S. Yan and Z. Zou, A Facet-Dependent Schottky-Junction Electron Shuttle in a $BiVO_4$ {010}-Au-Cu_2O Z-Scheme Photocatalyst for Efficient Charge Separation, *Adv. Funct. Mater.*, 2018, **28**, 1801214.